



# From micro-to macroscopic: Understanding optical properties in zinc-blend-derived materials $\text{Cu}_2\text{ZnYX}_4$ ( $X = \text{S, Se, Te, Y} = \text{Si, Ge, Sn}$ ) by means of the quantum chemical topology analysis



O. Mebkhout<sup>a</sup>, T. Ouahrani<sup>b, c, \*</sup>, A. Morales-Garcia<sup>d</sup>, B. Lasri<sup>a, c</sup>, J. Pilmé<sup>e, f</sup>,  
A.H. Reshak<sup>g, h</sup>

<sup>a</sup> Université Dr Tahar Moulay de Saïda, B.P. 138, Cité el Nasr, Saïda, 20000, Algeria

<sup>b</sup> École Préparatoire en Sciences et Techniques, BP 165 R.P., 13000, Tlemcen, Algeria

<sup>c</sup> Laboratoire de Physique Théorique, Université de Tlemcen, 13000, Tlemcen, Algeria

<sup>d</sup> Charles University in Prague, Faculty of Science, Department of Physical and Macromolecular Chemistry, Hlavova 2030, 128 40, Prague 2, Czech Republic

<sup>e</sup> Laboratoire de Chimie Théorique, UMR 7616 CNRS, UPMC Univ. Paris 06, Sorbonne Universités, Case Courier 137, 4 Place Jussieu, 75252, Paris Cedex05, France

<sup>f</sup> CNRS UMR 7616, 4 Place Jussieu, 75252, Paris Cedex 5, France

<sup>g</sup> New Technologies – Research Center, University of West Bohemia, Univerzitni 8, 306 14, Pilsen, Czech Republic

<sup>h</sup> Center of Excellence Geopolymer and Green Technology, School of Material Engineering, University Malaysia Perlis, 01007, Kangar, Perlis, Malaysia

## ARTICLE INFO

### Article history:

Received 15 July 2015

Accepted 31 August 2015

Available online 4 September 2015

### Keywords:

Ab initio calculation

Bonding analysis

Electronic population

Dipolar polarization

## ABSTRACT

Intensive calculations in the framework of the density functional theory (DFT) scheme have been carried out in order to predict accurately the dynamical stability and electronic properties of the zinc-blend-derived  $\text{Cu}_2\text{ZnYX}_4$  ( $X = \text{S, Se, Te, Y} = \text{Si, Ge, Sn}$ ) compounds. Emphasis is also placed on the optical properties of the defect chalcopyrite compounds. Advantages of the analysis of the topology of the electron localization function (ELF) to provide microscopic point of view of the chemical bonding in solids are illustrated. A relationship between polarization of bonds and origin-independent atomic contributions to electric dipoles in the  $\text{Cu}_2\text{ZnYX}_4$  ( $X = \text{S, Se, Te, Y} = \text{Si, Ge, Sn}$ ) defect chalcopyrite compounds is highlighted. In fact, what makes these compounds most interesting is a rich collection of S–Y long-distance bond paths. The ELF attractors do not systematically localize on the bond midpoint and their localization depends on electronegativity differences between the atoms forming the X–Y bond and on the nature of the chemical environment. Particularly, we show that the charge transfer remains generally the main contribution to the local bond dipole contribution. The compound which exhibits perturbed S lone pair is the more promising for nonlinear optical properties.

© 2015 Elsevier B.V. All rights reserved.

## 1. Introduction

In recent years, several studies have been devoted to the zinc-blend derived materials [1]. However, the origins of permanent and induced dipole moments in these systems, related to electric polarizabilities and other optical response properties, are still largely unknown. In 2001, Quemard et al. [2] have suggested that the concentration of electron lone pairs is the dominant factor in achieving large nonlinearities, and it has recently been confirmed

that the nonlinear refractive index increases with the most polarizable constituent. Moreover, it has been recently shown that a change in the electron lone-pair concentration modifies the energy gap in a way that it is impossible to determine whether a corresponding change in the nonlinearity is due to lone pairs or resonant enhancement [2].

In this work, we propose to highlight the relationship between polarization of bonds and lone pairs (microscopic point of view) and the macroscopic optical properties by means of the Quantum Chemical Topology (QCT). This methodology is based on a combined study of gradient fields of the electron density, namely the Atoms in Molecules Theory (AIM) [3–5] and the Electron Localization Function (ELF) [6,7]. Overall, the aim of this methodology is to answer general questions about the nature of chemical bonds or

\* Corresponding author. École Préparatoire en Sciences et Techniques, BP 165 R.P., 13000, Tlemcen, Algeria. Tel.: +213 43 20 18 24.

E-mail address: [tarik.ouahrani@yahoo.fr](mailto:tarik.ouahrani@yahoo.fr) (T. Ouahrani).

the reactivity of chemical compounds [8,9], but we focused more particularly our study on the polarity of bonds and lone pairs. To do so, a set of candidate crystalline compounds, namely  $\text{Cu}_2\text{ZnGeS}_4$ ,  $\text{Cu}_2\text{ZnGeSe}_4$ ,  $\text{Cu}_2\text{ZnGeTe}_4$ ,  $\text{Cu}_2\text{ZnSiS}_4$ ,  $\text{Cu}_2\text{ZnSiSe}_4$ ,  $\text{Cu}_2\text{ZnSiTe}_4$ ,  $\text{Cu}_2\text{ZnSnS}_4$ ,  $\text{Cu}_2\text{ZnSnSe}_4$  and  $\text{Cu}_2\text{ZnSnTe}_4$  have been studied. Among these systems, we carried out topological analyzes of three selected compounds, namely  $\text{Cu}_2\text{ZnSnS}_4$ ,  $\text{Cu}_2\text{ZnGeS}_4$  and  $\text{Cu}_2\text{ZnSiS}_4$ . Indeed, these materials are suspected to have an interesting polarizable behavior, namely a nonlinear behavior in their optical properties. Indeed, in this kind of compounds could played an crucial role in the structural distortions.

Overall, the minerals under study belong to the  $A_2^I B^II C^IV X_4^{VI}$  compound family structured in different ordered superstructures on the basis of zincblende, with three different cations and 8 cationic sites [1]. Such quaternary semiconductor systems are promising for photovoltaic applications [10–12]. They also aroused much interest in the field of nonlinear optics (NLO) since their unusual nonlinear optical indices have been noticed [12]. Unfortunately, there is a cruel lack of experimental nonlinear susceptibility data for defect chalcopyrite phases, mainly due to the difficulty of growing sufficiently large single crystals. In this perspective, we hope that first-principles calculations, relying on unambiguous chemical information, may help to pinpoint the benchmarks that make these compounds good candidates for application in the nonlinear fields. The importance of polarizabilities and hyperpolarizabilities is widely recognized since they are needed in the study of the nonlinear optical properties of atomic and molecular systems [13–15]. Given the overall closeness in chemistry and a tricky structural relation between the dipolar contribution of bonds into the entitled compounds, we can trace how the features of different spatial confinement of bond and charges emerge and give rise to the hyperpolarizability trend.

We organize the paper as follows: After a presentation of the methodology in Section 2, Section 3 will refers to the technical side of calculations. Section 4 is divided in two more sections. The first, briefly outlines the structural and dynamical properties of the investigated compounds. The second one gives detailed study of electronic, bonding and optical properties of the studied materials. We will also rationalize here our findings in terms of simple ideas. Finally, Section 5 will present our conclusions and some future prospects.

## 2. Theory

The Electron Localization Function (ELF) was originally designed by Becke and Edgecombe to identify localized electronic groups in atomic and molecular systems [6] in a Hartree–Fock framework. From this seminal definition, several interpretations were given, for example in the context of Markovian processes [16,17]. However, the most intuitive interpretation is that proposed by Savin et al. [18] in the DFT framework for which ELF can be understood as a local measure of the excess of local kinetic energy of electrons due to the Pauli principle,  $t_p(\vec{r})$ . This quantity is computed by subtracting the bosonic contribution,  $|\nabla\rho(\vec{r})|^2/8$ , from the kinetic energy density of the system,  $t(\vec{r})$ . Re-scaling it with respect to the homogeneous electrons gas like in the original definition provides the core of ELF,  $\chi(\vec{r})$ :

$$\chi(\vec{r}) = \frac{t_p(\vec{r})}{t_w(\vec{r})} = \frac{t(\vec{r}) - \frac{1}{8} \frac{|\nabla\rho(\vec{r})|^2}{\rho}}{c_F \rho^{5/3}(\vec{r})} \quad (1)$$

where  $c_F$  is the Fermi constant. According to this definition, the regions of electron pairing would have a small  $\chi$  value. In order to

inverse this relationship and map it in a closed interval, the final function was defined as follows:

$$ELF(\vec{r}) = \frac{1}{1 + \chi^2(\vec{r})} \quad (2)$$

It can be easily seen that ELF runs from 0 to 1, and equals to 0.5 in the uniform electron gas. Note that this expression has been also defined a quasirelativistic context [19].

Based on the theory of gradient dynamical systems, the quantum chemical topology is a combined analysis of gradient fields of the electron density (AIM theory) and the ELF functions. This methodology is an interesting tool to overcome the complexity of molecular orbital analysis due to their delocalized character. This analysis provides non-overlapping regions, termed basins (noted  $\Omega$ ), which are stable manifolds of the attractors (maxima) (this would be like partitioning a set of mountains by the valleys) [3,7,9]. While AIM topology is only atomic, the ELF topology gives a non-atomic partition into localized electron pairs regions. A synaptic order of a valence ELF basin is the number of core basins with which they share a common boundary (zero-flux surface). Each valence basin is then presented with a chemical meaning in agreement with the Lewis theory: monosynaptic basin, labeled  $V(A)$ , in the lone-pair region of A atom; disynaptic basin, labeled  $V(A, B)$ , of two-center A–B bonds. Overall, the spatial location of basins closely match the VSEPR domains [20].

Integrated properties can be determined by integration of the electron density over the basin volumes. Most commonly, basin volumes and populations (noted  $N$ ) are used in order to rationalize the bonding schemes in molecules or in solids. The atomic AIM charge of a topological atom,  $q(\Omega)$ , can be calculated by subtracting the atomic population from the valence of each atom,  $Z_{val}$ . The properties of these basins have a chemical meaning inherited from the partition, so that the integration of the density over a ELF basin associated with a  $V(A, B)$  basin, can be understood as the bond population of the two-center A–B bond. From a microscopic point of view, a way to compute the basin polarization of any covalent or dative bond can be performed using a combination of ELF and AIM topologies. Indeed, Raub and Jansen [21] have introduced a bond polarity index  $p_{XY}$  defined for a disynaptic basin  $V(A, B)$  as follows:

$$p_{XY} = \frac{A|\bar{N}[V(A, B)] - B|\bar{N}[V(A, B)]}{A|\bar{N}[V(A, B)] + B|\bar{N}[V(A, B)]} \quad (3)$$

where  $A|\bar{N}[V(A, B)]$  and  $B|\bar{N}[V(A, B)]$  provide the AIM contributions of A and B, respectively, to the total population of  $V(A, B)$ . Thus, a strong polarized bond yields an index close to 1.

Moreover, it has been shown that the AIM basin polarization can be evaluated by means of the magnitude of the dipolar electrostatic moment (noted  $|\mathbf{M}_1|$ ) [4,5,22]. Note that recently, this methodology has been also adapted to the ELF topology [8]. The components of the  $|\mathbf{M}_1|$  are calculated as follows:

$$\mathbf{M}_{1,x}(\Omega) = - \int_{\Omega} (x - X_c)\rho(\mathbf{r})d\mathbf{r}^3 \quad (4)$$

$$\mathbf{M}_{1,y}(\Omega) = - \int_{\Omega} (y - Y_c)\rho(\mathbf{r})d\mathbf{r}^3 \quad (5)$$

$$\mathbf{M}_{1,z}(\Omega) = - \int_{\Omega} (z - Z_c)\rho(\mathbf{r})d\mathbf{r}^3 \quad (6)$$

where  $X_c, Y_c, Z_c$  are the cartesian coordinates of the nuclear centers.  $|\mathbf{M}_1|$  is then calculated as the square root of the sum of squared

components. Because of the invariance of  $|\mathbf{M}_1|$  with respect to the orientation of the system of axis, it is then possible to compare the polarization lone pairs in different chemical environment [23].

A goal of this article is to highlight the relationship between polarization of charge distributions (microscopic point of view) and the macroscopic optical properties related to the total energy  $E$  of a perturbed system.  $E$  can be expressed in powers of the field components (denoted by indices  $t, u, v \dots$ )

$$E(\varepsilon) = E(0) - \sum_t \mu_t \varepsilon_t - \frac{1}{2!} \sum_{tu} \alpha_{tu} \varepsilon_t \varepsilon_u - \frac{1}{3!} \sum_{tuv} \beta_{tuv} \varepsilon_t \varepsilon_u \varepsilon_v - \frac{1}{4!} \sum_{tuvw} \gamma_{tuvw} \varepsilon_t \varepsilon_u \varepsilon_v \varepsilon_w + \dots \quad (7)$$

where derivatives

$$\mu_t = - \left. \frac{\partial E}{\partial \varepsilon_t} \right|_0 \quad (8)$$

$$\alpha_{tu} = - \left. \frac{\partial^2 E}{\partial \varepsilon_t \partial \varepsilon_u} \right|_0 \quad (9)$$

$$\beta_{tuv} = - \left. \frac{\partial^3 E}{\partial \varepsilon_t \partial \varepsilon_u \partial \varepsilon_v} \right|_0 \quad (10)$$

$$\gamma_{tuvw} = - \left. \frac{\partial^4 E}{\partial \varepsilon_t \partial \varepsilon_u \partial \varepsilon_v \partial \varepsilon_w} \right|_0 \quad (11)$$

represent optical properties of increasing order, respectively: the permanent electric dipole moment  $\mu$  (vector), the polarizability  $\alpha$  (tensor of rank 2), the 1st hyperpolarizability  $\beta$  (tensor of rank 3) and the 2nd hyperpolarizability  $\gamma$  (tensor of rank 4).

### 3. Computational modelling

In order to assure the accuracy of the global investigation (electronic and optical properties), we have followed first-principles methodologies based on the density functional theory as implemented in the (all-electron full potential linearized augmented-plane wave) FP-LAPW<sub>ELK</sub> [24] package. We used the ability of ELK code to do a full optimization of the defect chalcopyrite structure. A satisfactory degree of convergence was achieved by considering a number of FP-LAPW basis functions up to  $R_{MT} \times K_{max}$  equal to 8 (where  $R_{MT}$  is the minimum radius of the muffin tin spheres and  $K_{max}$  gives the magnitude of the largest  $\mathbf{k}$  vector in the plane wave expansion). To keep the same degree of convergence for all the lattice constants studied, we kept the values of the sphere radii and  $K_{max}$  constant over all the range of lattice spacing considered. However, Fourier expanded charge density was truncated at  $G_{max} = 12$ . As a general guideline, structural and geometrical optimization tasks were calculated under the hybrid generalized gradient approximation (PBEsol) using Perdew-Burke-Ernzerhof functional revised for solid [25]. Whereas the modified Becke and Johnson (mBJ) potential [26] was used for electro-optic investigation. The Engel-Vosko-GGA (EV-GGA) formalism [27] was also applied to optimize the corresponding potential for calculating the band structure and optical properties.

For the calculation of local measures (ELF, AIM and dipolar polarization), we have used the Vienna *ab initio* simulation package (VASP) [28]. We used the projector augmented wave (PAW) all-electron description of the electron-ion-core interaction [28]. Total energy minimization was obtained by calculating Hellmann-

Feynman forces and the stress tensor. The optimization of lattice parameters and the relaxation of atomic positions have been done by the conjugate gradient method. The atomic relaxation was stopped when forces acting on atoms were less than 0.01 eV/Å. The cut-off was found to be adequate for the structural as well as for the electronic structure. It is not observed statistically significant changes in the key parameters when the energy cut-off is increased from 550 to 600 eV. The  $10 \times 10 \times 8$  grid of Monkhorst-Pack points was used. The convergence in the total energy of the unit cell was better than 1 meV/atom. All the topological analyses were carried out with the TopCHEM package [29] using very fine grids (AIM and ELF) of size  $216 \times 216 \times 430$ .

## 4. Results and discussions

### 4.1. Ground state properties

Theoretically, the zinc-blend-derived kesterite (KS) structures [space group  $\bar{1}\bar{4}$ , Fig. 1(b)] have been shown to be the most stable structures for the  $\text{Cu}_2\text{Zn-IV-VI}_4$  systems due to the small strain energy and more negative Madelung energy. The zinc-blend-derived stannite (ST) structures [space group  $\bar{1}\bar{4}2m$ , Fig. 1(c)] are slightly less stable than the KS structures, and the KS and ST ordering may coexist in the synthesized samples. But according to the works of Pamplin [30]  $\text{Cu}_2\text{Zn-IV-VI}_4$  systems can also exist in the defect chalcopyrite (DC) structures [space group  $\bar{1}\bar{4}$ , Fig. 1(a)], subject of this study. Due to their band gap around 1.5 eV, it is undoubtedly proven that KS and ST structures are promising for solar cells applications [31]. But DC system seems to have lower values of band gap, which make it rather more favorable for NLO applications.

We have completed extensive numerical analyses in order to secure stability of the computed zero pressure equilibrium values of the tow structures (KS and DC). We convert the calculated energy-volume ( $E, V$ ) into static and finite-temperature pressure-volume ( $p, V$ ) isotherms using numerical and analytical procedures coded in the GIBBS2 program [32]. Thermal contributions are included by means of a non-empirical quasi-harmonic Debye-like model. This approach only needs the set of ( $E, V$ ) points and the calculated static bulk modulus to evaluate thermodynamic properties at different temperatures. At each volume, the internal parameters are optimized to give the minimum total energy following a conjugate gradient algorithm. This procedure provides the dependence of the total energy on volume, which serves as an input for the determination of the equation of states (EOS). The athermal (static) computed lattice parameters for the 18 compounds in their respective structures [33] are displayed in Table 1. As the KS structures of our compounds are widely investigated experimentally [34–38] and theoretically [33] we can have an opportunity to compare our results with them. So, to prove the accuracy of our calculation, we fed Table 1 with the optimized parameter of the KS structure. As regards the comparison with available experimental data at room temperature, it is to be noticed that theory yields a closer results compared to the data values quoted in Refs. [33–37].

Calculating the phonon spectra is arguably most successful technical way for the prediction of the stability of the solid. However, the computational cost can be too large. To achieve the proof of the stability of any material, researchers make use to evaluate the Born stability criteria which ensures that the lowest frequency acoustic branches at the  $\Gamma$ -point in the phonon dispersion have all positive slopes. This criteria can be calculating by diagonalizing the  $C_{ij}$  matrix;  $C_{ij}$  being the non-zero elastic stiffness. The calculating elastic stiffness have been calculated and listed in Table 1. We can evaluate the Born stability criteria:  $C_{11} > |C_{12}|$ ,  $(C_{11} + C_{12})C_{33} > 2C_{13}^2$ ,  $C_{44} > 0$

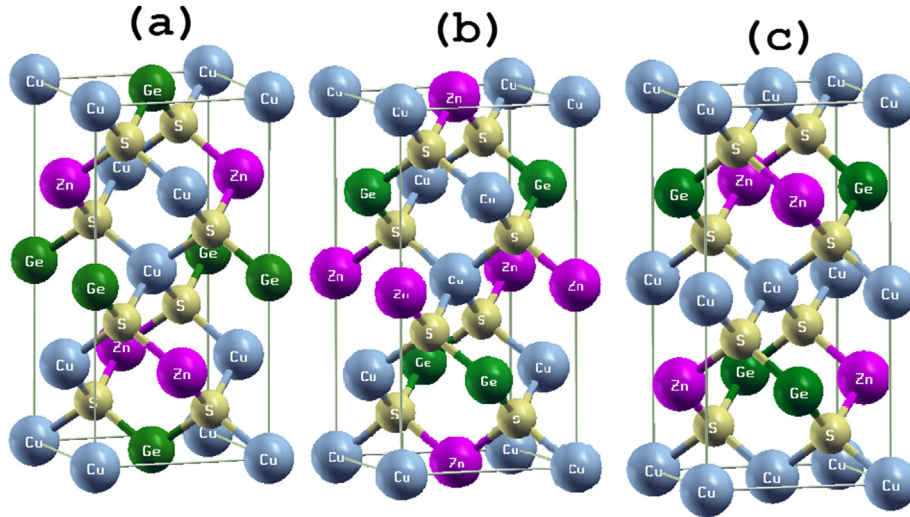


Fig. 1. Structural representation of the (a) defect chalcopyrite ( $sp \bar{I}4$ ) (b) k esterite ( $sp \bar{I}4$ ) and (c) stannite ( $sp \bar{I}4 2m$ ).

and  $C_{66} > 0$ . As a qualitative check of Table 1, we can assess these criteria of each predicted defect chalcopyrite and k esterite compounds and confirm their mechanical stability.

Even though the inner strain component is particularly difficult to calculate shear constants ( $C_{44}$  and  $C_{66}$ ). Our calculated elastic constants appear to be comparable to those quoted from available theoretical values in Refs. [39–41]. Maybe the small difference is due to the used of methodologies and XC exchange: pseudo potential (GGA) in Refs. [39–41] and FP-LAPW (PBESol) in this work. To check the internal consistency of our elastic constants we can compare the bulk modulus reported on Table 1 with an equivalent combination of the  $C_{ij}$ 's. Bulk modulus should be bound from above

by the Voigt approximation,  $B_V$  (uniform strain assumption), and from below from the Reuss approximation,  $B_R$  (uniform stress), which happens to be formally equivalent to the single crystal.

The Voigt (V) [42] and Reuss (R) [43] limits for the bulk modulus ( $B$ ) and shear modulus ( $G$ ) are [44]:

$$B = \frac{(C_{11} + C_{12})C_{33} - 2C_{13}^2}{C_{11} + C_{12} + 2C_{33} - 4C_{13}} \quad (12)$$

$$B_V = \frac{1}{9} \{2(C_{11} + C_{12}) + C_{33} + 4C_{13}\} \quad (13)$$

Table 1

Calculated lattice parameters ( $a$  and  $c$  in Angstrom), bulk modulus ( $B_0$  in GPa) and elastic constants ( $C_{ij}$  in GPa) of the investigated compounds in DC and KS structures. From the  $C_{ij}$  Voigt ( $B_V$ ) and Reuss ( $B_R$ ) modulus given in GPa unite.

	$a$	$c$	$B_0$	$C_{11}$	$C_{12}$	$C_{13}$	$C_{33}$	$C_{44}$	$C_{66}$	$B_R$	$B_V$
$Cu_2ZnGeS_4$ (DC)	5.4374	10.785	70.184	101.18	55.86	54.02	101.51	44.70	47.95	70.182	70.186
(KS) this work	5.359	10.646	78.365	119.88	70.18	50.65	123.64	51.68	56.36	78.247	78.483
Refs. [33–37]	5.341	10.5111	–	–	–	–	–	–	–	–	–
$Cu_2ZnGeSe_4$ (DC)	5.6673	11.286	63.709	103.53	34.10	53.89	82.58	33.15	35.97	63.708	63.711
(KS) this work	5.666	11.277	71.498	88.48	55.14	67.94	87.45	38.39	38.17	71.168	71.827
Refs. [33–37]	5.606	11.0438	–	–	–	–	–	–	–	–	–
$Cu_2ZnGeTe_4$ (DC)	6.0878	12.123	45.619	61.01	31.31	48.84	53.82	27.03	29.69	43.36	48.202
(KS) this work	6.08709	12.123	19.006	30.13	16.11	11.79	31.53	13.46	24.70	18.99	19.02
$Cu_2ZnSiS_4$ (DC)	5.3083	10.445	92.292	130.58	83.40	68.04	131.55	47.42	52.18	92.18	92.405
(KS) this work	5.309	10.451	93.259	149.20	45.47	83.65	115.62	49.59	33.32	93.234	93.286
Refs. [33–37]	5.309	10.384	–	–	–	–	–	–	–	–	–
$Cu_2ZnSiSe_4$ (DC)	5.6234	11.089	77.850	108.04	62.31	64.08	103.67	39.21	38.90	77.844	77.586
(KS) this work	5.61835	11.0897	79.469	127.34	43.46	66.98	105.74	41.11	33.83	79.465	79.473
Refs. [33–37]	5.607	10.956	–	–	–	–	–	–	–	–	–
$Cu_2ZnSiTe_4$ (DC)	6.0358	11.969	50.805	87.58	24.16	40.99	69.83	31.80	37.61	50.804	50.806
(KS) at 293 K Ref. [38]	5.9612	11.7887	–	–	–	–	–	–	–	–	–
(KS) this work	6.04495	11.99181	50.811	91.67	29.43	34.59	77.34	30.38	38.35	50.743	50.879
$Cu_2ZnSnS_4$ (DC)	5.4679	10.936	80.241	115.16	71.79	58.98	113.53	43.81	45.99	80.111	80.370
(KS) Refs. [33–37]	5.427	10.8757	–	–	–	–	–	–	–	–	–
(KS) this work	5.468	10.933	72.802	116.67	30.84	67.98	90.36	40.94	40.58	72.357	73.033
(KS) VASP (PAW) Ref. [39]	5.477	10.941	67.8	91.8	55.7	55.8	92.0	41.8	41.2	–	–
(KS) CASTEP (GGA-WC) Ref. [41]	5.393	10.797	78.439	105.582	67.343	67.528	103.244	49.779	50.101	–	–
$Cu_2ZnSnSe_4$ (DC)	5.7636	11.549	67.667	110.80	44.82	50.91	94.79	32.94	36.00	67.589	67.743
Refs.[33, 34, 35, 36, 37]	5.693	11.329	–	–	–	–	–	–	–	–	–
(KS) this work	5.7641	11.525	66.757	111.38	45.79	47.50	97.42	31.63	37.53	66.654	66.859
(KS) VASP (PAW) Ref. [40]	5.770	11.533	55.7	75.9	46.6	45.4	74.8	33.5	33.7	–	–
(KS) CASTEP (GGA-WC) Ref. [41]	5.642	11.303	65.706	90.721	57.352	57.174	90.274	42.71	41.729	–	–
$Cu_2ZnSnTe_4$ (DC)	6.1593	12.306	46.553	56.36	30.78	48.22	46.77	26.01	36.49	47.116	45.991
(KS) this work	6.1834	12.363	41.552	75.47	24.56	29.59	57.31	25.35	33.07	41.353	41.751

$$B_R = \frac{C^2}{M} \quad (14)$$

where  $C^2 = (C_{11} + C_{12})C_{33} - 2C_{13}^2$  and  $M = C_{11} + C_{12} + 2C_{33} - 4C_{13}$ .

It is showed Table 1, that in obtained values of bulk modulus from the equation of states for the KS and DC type respectively are close to the calculated values from the single crystal elastic constants ( $B_V, B_R$ ), which enhances the accuracy of present calculations.

#### 4.2. Bonding analysis

The DC and KS compounds being studied are tetrahedrally coordinated; they possess a four tetravalent-VI ( $X = S, Se, Te$ ) anions and the  $s$ -states of these atoms can be treated as filled core states. However, the  $p$ -states of anions and  $s$ -states of ( $Y = Si, Ge, Sn$ ) cations, strongly interact and form the bonding and anti-bonding bands, giving rise to an unoccupied band near the Fermi level. Our focus here is to understand the nature of the electronic properties of the compounds and its relation to the inter-atomic bonds, critically examining the valency of the nominally pentavalent cation ( $ns^2 np^2$  shells of  $Y$ ) and the role of its lone pair ( $ns^2$ ) in the band-gap formation. Thus, in an attempt to identify the key features of the bonding and structure that strongly couple with the electronic structure near the Fermi level. We can discuss our results within the energy band structure. We have used in this study the EV-GGA as well as mBJ approaches in order to improve the calculated band gap. Thereby, the calculated values within mBJ are considerably in good agreement with the theoretical results and experimental measures quoted from Ref. [45]. A glance at Table 2 can inform us that due to small value of the energy gaps, the materials under investigation are prerequisite for photocatalysis applications. We have supplemented our analysis with an investigation of the partial decomposition of states (PDOS). Since the patterns of the PDOS are almost the same for all studied compounds, we have chosen to present in Fig. 2 only three densities namely of the  $Cu_2ZnGeS_4$ ,  $Cu_2ZnSiS_4$  and  $Cu_2ZnSnS_4$  DC compounds. Fig. 2 reveals clearly that the conduction band is originated from the antibonding  $\pi$  interaction between the  $X$ - $p$  and the  $Y$ - $sp$  orbitals. However, the highest occupied molecular orbitals (HOMO) are primarily derived from nonbonding  $Y$   $2p$  orbitals, and the lowest unoccupied molecular orbitals (LUMO) are primarily derived from  $X$   $3p$  orbitals. Thus, the HOMO–LUMO energy gap can be seen as a measure of the energy of the charge transfer from the  $X$  orbitals to the  $Y$  orbitals. The orbitals analyzed in this part are being the most involved in the permitted transitions because they construct the shape of the polarizability.

In general, polarizability correlates with the interaction between electrons and the nucleus. The amount of electrons in a molecule affects how tight the nuclear charge can control the overall charge distribution. Atoms with less electrons will have smaller, denser electron clouds, as there is a strong interaction between the few electrons in the atoms' orbitals and the positively charged nucleus. There is also less shielding in atoms with less electrons contributing to the stronger interaction of the outer electrons and the nucleus. With the electrons held tightly in place in these smaller atoms, these atoms are typically not easily polarized by external electric fields. In contrast, large atoms with many electrons, such as negative ions with excess electrons, are easily polarized. These atoms typically have very diffuse electron clouds and large atomic radii that limit the interaction of their external electrons and the nucleus.

A systematic study of the second harmonic generation properties in the defect chalcopyrite compounds seems to be lacking. Here we will provide a minimal set of the main results of nonlinear

**Table 2**

Calculated band gap energy compared with experimental and theoretical data quoted from Ref. [45].

	$E_g$ (EVGGA)	$E_g$ (mBJ)	Experiments quoted from Ref. [45]
$Cu_2ZnGeS_4$ (DC)	0.65	1.01	–
(KS)	–	1.20	–
Ref. [45] (KS)	–	1.51	2.07, 2.13
$Cu_2ZnGeSe_4$ (DC)	0.18	0.52	–
(KS)	–	0.52	–
Ref. [45] (KS)	–	0.84	1.498, 1.66
$Cu_2ZnGeTe_4$ (DC)	0.05	0.33	–
(KS)	–	0.12	–
Ref. [45] (KS)	–	0.45	–
$Cu_2ZnSiS_4$ (DC)	1.93	2.33	–
(KS)	–	2.34	–
Ref. [45] (KS)	–	2.55	2.97, 3.07, 3.25
$Cu_2ZnSiSe_4$ (DC)	0.94	1.34	–
(KS)	–	1.38	–
Ref. [45] (KS)	–	1.65	2.1 ~ 2.3
$Cu_2ZnSiTe_4$ (DC)	1.36	1.48	–
(KS)	–	1.07	–
Ref. [45] (KS)	–	1.10	1.47
$Cu_2ZnSnS_4$ (DC)	0.41	0.63	–
(KS)	–	0.65	–
Ref. [45] (KS)	–	0.91	1.46, 1.50, 1.51
$Cu_2ZnSnSe_4$ (DC)	0.05	0.28	–
(KS)	–	0.28	–
Ref. [45] (KS)	–	0.54	1.0, 1.40 ~ 1.65
$Cu_2ZnSnTe_4$ (DC)	0.13	0.31	–
(KS)	–	0.32	–
Ref. [45] (KS)	–	0.47	–

optical properties. A better authoritative account of the theory may be found in Refs. [46–48], and works cited therein. Our treatment closely follows that found in Ref. [49]. As a starting point, we display as a function of energy the absolute values of the dominant components of the second order susceptibility  $\chi^{(2)}$  of the studied DC structure in Fig. 3. Some information may be gained by examining this plot: the compounds with atomic constituent of germanium or tin seems to have more dominant nonlinear optical properties. Let us now examine the most significant aspects of our predictions.

The AIM volumes and charges of selected DC compounds  $Cu_2ZnGeS_4$ ,  $Cu_2ZnSiS_4$  and  $Cu_2ZnSnS_4$  are reported in Table 4. As expected, S shows a large negative charge (close to  $-1.30e$ ) while the charges of Ge, Si and Sn cations appear superior to those of the Cu and Zn ones. Interestingly, this statement corresponds to the case where the Fig. 3 shows a large contribution of the  $|\chi^{(2)}|$ . Moreover, it is worth noting that  $q(S)$  remains rather unchanged whatever the considered compound.

It has been shown that further insights into the nature of chemical bonds can be gained by means of the ELF topological analysis in solids. [50,51], we focus here our analysis on the chemical environment of sulfur. Fig. 4 displays the ELF localization domains of the  $Cu_2ZnSiS_4$  compound.

It worth noting that the ELF topology of other selected DC species, namely  $Cu_2ZnGeS_4$  and  $Cu_2ZnSnS_4$ , is quite similar. Fig. 4 reveals that the valence of S splits into four basins tetrahedrally distributed around the S center and located along the bond axis: two equivalent monosynaptic basins  $V(S)$  located along the S–Cu axis, one basin  $V(S)$  located along the S–Zn axis and a fourth basin  $V(S, Si)$  showing a bonding character. Moreover, Fig. 4 shows that the domain of S topological atom is strongly polarized along the S–Si axis and largely encompasses the four ELF domains without overlapping with near atoms (Cu, Zn and Si). This ELF topology reveals structural changes taking place, showing that atomic sphericity of S is substituted by deformed ELF polarized basins. Moreover, the lack of additional disynaptic basins  $V(S, Cu)$  or  $V(S,$

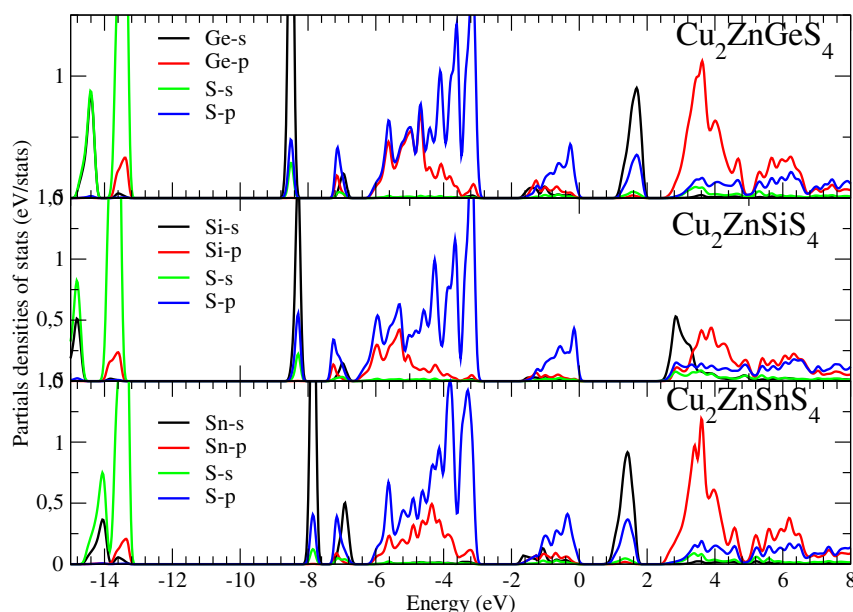


Fig. 2. Partial densities of states the DC  $\text{Cu}_2\text{ZnGeS}_4$ ,  $\text{Cu}_2\text{ZnSiS}_4$  and  $\text{Cu}_2\text{ZnSnS}_4$  compounds.

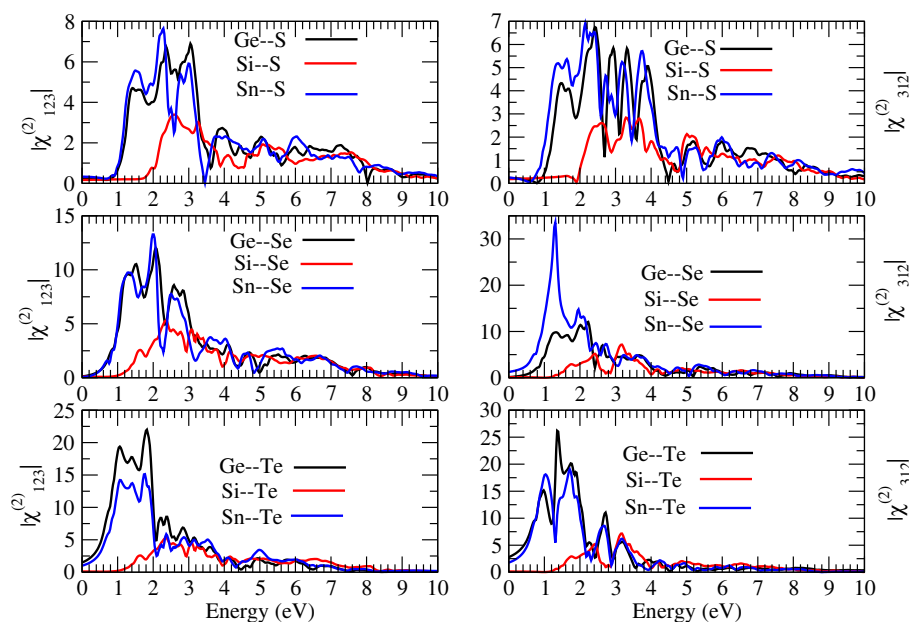


Fig. 3. Absolute value of the second order susceptibility  $\chi^{(2)}$  of the studied DC compounds.

Table 3

First ( $\chi^{(1)}$ ), second ( $\chi^{(2)}$ ) and third ( $\chi^{(3)}$ ) order susceptibilities of the  $\text{Cu}_2\text{ZnGeS}_4$ ,  $\text{Cu}_2\text{ZnSiS}_4$  and  $\text{Cu}_2\text{ZnSnS}_4$  compounds in their DC structure. According to the relation 7, we have  $1 + \chi^{(1)} = 1 + 4\pi\alpha/V$ ,  $\chi^{(2)} = 2\pi\beta/V$  and  $\chi^{(3)} = 2\pi\gamma/(3V)$ .  $V$  is the volume of the cell; all susceptibilities are in a.u. unite.

	$\chi_{xx}^{(1)}$	$\chi_{zz}^{(1)}$	$\chi_{xxz}^{(2)}$	$\chi_{xyy}^{(2)}$	$\chi_{yzz}^{(2)}$	$\chi_{xxxx}^{(3)}$	$\chi_{xxyy}^{(3)}$	$\chi_{xxyy}^{(3)}$	$\chi_{xxzz}^{(3)}$	$\chi_{xyyy}^{(3)}$	$\chi_{yyyy}^{(3)}$	$\chi_{yyzz}^{(3)}$	$\chi_{zzzz}^{(3)}$
$\text{Cu}_2\text{ZnGeS}_4$	2.75	2.81	1.98	-4.06	-1.98	2.73	-0.01	1.35	1.32	0.02	2.73	1.32	3.08
$\text{Cu}_2\text{ZnSiS}_4$	2.53	2.57	1.62	-3.45	-1.62	2.02	-0.02	1.02	1.05	0.02	2.02	1.05	2.20
$\text{Cu}_2\text{ZnSnS}_4$	2.60	2.63	1.71	-4.14	-1.71	2.91	-0.02	1.62	1.38	0.02	2.91	1.38	3.02

Zn) confirms the main ionic character of Cu–S and Zn–S bonds whereas the presence of the disynaptic V(S, Si) basin suggests a non-negligible covalent character of the S–Si bond. Nevertheless, the ELF population analysis, provided in Table 5, shows a more subtle scheme.

As expected, the ELF population of V(S) basins (lone pairs) are always close to 2 electrons and the volumes of these basins remain almost unchanged whatever the considered DC compound. The population of the V(S, Y) basin is also close to 2 electrons which typically corresponds to a single covalent bond [9]. Thus, regarding

**Table 4**

AIM volumes ( $\text{bohr}^3$ ), charges  $q$  (electrons) and  $|M_1|$  (electrons.bohr) of  $\text{Cu}_2\text{ZnYS}_4$  ( $Y = \text{Si, Ge, Sn}$ ) compounds.

	$\text{Cu}_2\text{ZnSiS}_4$			$\text{Cu}_2\text{ZnGeS}_4$			$\text{Cu}_2\text{ZnSnS}_4$		
	Vol.	$q$	$ M_1 $	Vol.	$q$	$ M_1 $	Vol.	$q$	$ M_1 $
S	167	-1.31	61	184	-1.30	62	183	-1.31	62
Y	10	3.59	4.2	11	3.55	4.4	10	3.87	1.2
Zn	100	0.95	78	98	0.89	76	100	0.92	75
Cu	100	0.51	73	106	0.51	80	104	0.48	80

the covalent character of the bond, the S–Si bond seems to be slightly strongest than other ones  $V(S, Y)$  since its population is larger than the other ones.

#### 4.3. Polarizabilities and their derivatives

In this subsection, the coupled perturbed Hartree–Fock performed at frequencies method [52] for computing electronic nonlinear optical properties of periodic systems has been applied to calculate the polarizability  $\alpha$  ( $1 + \chi^{(1)} = 1 + 4\pi\alpha/V$ ) tensor of rank 2), the 1st hyperpolarizability  $\beta$  ( $\chi^{(2)} = 2\pi\beta/V$  tensor of rank 3) and the 2nd hyperpolarizability  $\gamma$  ( $\chi^{(3)} = 2\pi\gamma/(3V)$  tensor of rank 4). Although the coupled perturbed Hartree–Fock method gives satisfactory results, it requires a supercell to be defined, while keeping the periodicity along the applied field direction. The dimension of the studied system is thus very quickly limiting in terms of expansiveness in time and computational requirements. So a first-principles estimation of all of the third-order nonlinear susceptibility of the 9 DC compounds would be a rather cumbersome task, which is out of the scope of this work. Instead, we have chosen the ( $\text{Cu}_2\text{ZnGeS}_4$ ,  $\text{Cu}_2\text{ZnSiS}_4$  and  $\text{Cu}_2\text{ZnSnS}_4$ ) one to do this task (see Table 3), because they are informative enough for considering the subject of our investigation. The main remark from Table 3 emphasizes that high  $\chi^{(3)}$  values are related to the bonding of the compound, and that the polarization along  $z$  are much more favorable direction. This is attributed to an exceptionally strong nonlocality of the electronic polarization, that is, assuming

**Table 5**

ELF population analysis of  $\text{Cu}_2\text{ZnYS}_4$  ( $Y = \text{Si, Ge, Sn}$ ) compounds.  $\bar{N}$  in electrons, volume in Refs.  $\text{bohr}^3$ ,  $p_{XY}$  is the bond polarity index. The numbering of basins is given in agreement with Fig. 4.

Basin	$\text{Cu}_2\text{ZnSiS}_4$			$\text{Cu}_2\text{ZnGeS}_4$			$\text{Cu}_2\text{ZnSnS}_4$		
	Vol.	$\bar{N}$	$p_{XY}$	Vol.	$\bar{N}$	$p_{XY}$	Vol.	$\bar{N}$	$p_{XY}$
$V(S, Y)$	41	1.92	0.86	41	1.62	0.87	48	1.84	0.94
$V(S)_1$	62	1.73		68	1.80		60	1.71	
$V(S)_2$	56	1.87		64	1.97		59	1.91	
$V(S)_3$	63	1.89		66	2.02		61	1.93	

that the electric field applied at a given point would induce a dipole moment not only at the very point but in the vicinity of this point.

At this stage, the fundamental question of the polarity of the S–Y bonds deserves a special attention. The atomic charge of Y slightly increases from 3.59e(Si) to 3.87e(Sn) (see Table 4) in reasonable agreement with the electronegativity differences. In contrast, the charges of ions Zn (0.95e), Cu (0.5e) and S (–1.30e) remain quite unchanged in all compounds. This trend is confirmed by the dipolar polarization ( $|M_1|$ ) which is large and quite unchanged for Cu, Zn. In the case of Y,  $|M_1|$  is small and thus, this clearly indicates a very weak atomic polarization meaning that the topological atom is undisturbed by its chemical environment. This can be also understood as a almost negligible charge transfer from Y to the sulfur atom. Table 5 gives the ELF bond polarity index  $p_{XY}$  for each  $V(S, Y)$  bonding basin ( $Y = \text{Si, Ge, Sn}$ ). The values of  $p_{XY}$  are always upper than 0.85. This result is in agreement with the AIM analysis (charges and  $|M_1|$ ) because it reflects the strong polarization of the S–Y bond, the main atomic contribution of the  $V(S, Y)$  population coming from the sulfur atom. This trend is also common to DC and KS species: the presence of Si, Ge or Sn cations does not affect the properties of S. Se and Te probably should display a quite similar behavior. In a series, from Si to Sn, the bond polarity index increases in agreement with the electronegativity differences. In other words, these analyzes confirm that the S–Y interaction can be view as a S lone pair lightly perturbed by the chemical environment.

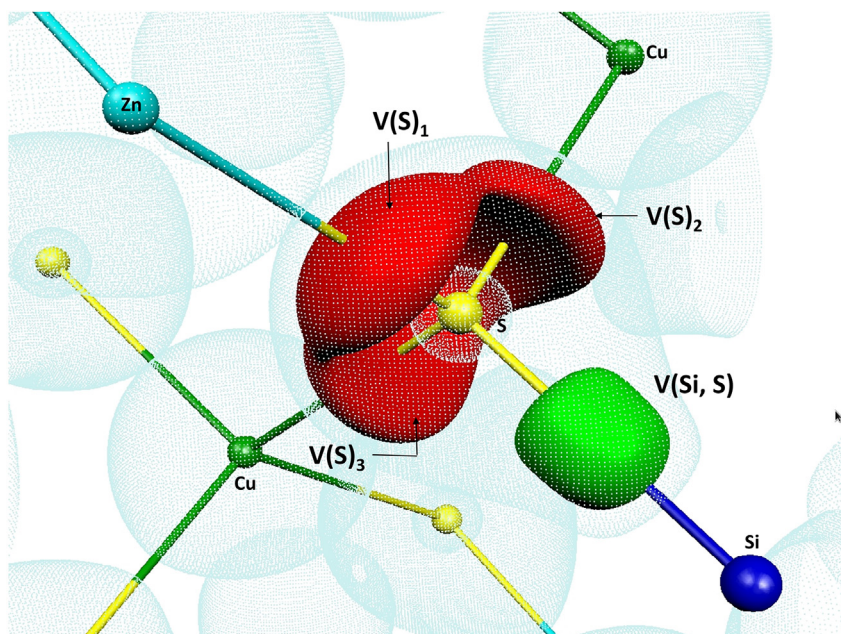


**Fig. 4.** ELF localization domains (ELF = 0.84) of  $\text{Cu}_2\text{ZnSiS}_4$  compound. **Color code:** green: bonding basin  $V(S, \text{Si})$ , red: valence basins  $V(S)$ . **Light blue dots:** contour map of the electron density ( $\rho = 0.07 \text{ e.Bohr}^{-3}$ ). (For interpretation of the references to color in this figure legend, the reader is referred to the web version of this article.)

## 5. Conclusion

In order to unravel the origin of optical properties of the  $\text{Cu}_2\text{ZnYX}_4$  ( $X = \text{S, Se, Te, Y} = \text{Si, Ge, Sn}$ ) compounds, we have used a combination of the electron localization function (ELF) analysis and density functional theory DFT methodology. Firstly, we have addressed a global description of the zero Kelvin temperature of structural and dynamical properties of the studied compounds. Given the realization of the Born criteria of the elastic constants for the DC and KS structures, we can confirm the stability of the  $\text{Cu}_2\text{ZnYX}_4$  in these phases. We have dressed a systematic study on electronic and optical properties of the selected DC  $\text{Cu}_2\text{ZnSnS}_4$ ,  $\text{Cu}_2\text{ZnGeS}_4$  and  $\text{Cu}_2\text{ZnSiS}_4$  compounds. The finding results reveal their capacity as nonlinear device.

Secondly, the ELF topological tools has proved to be versatile enough to be applied to track the volume and electronic population of the lone pair and covalent bonding of the selected compounds. In Fact, in this formalism, a balance between covalent and weak ionic chemical behavior has been highlighted: the compound with the Si cation is the more covalent with a localization of electron shared with the X anions. The polarization contribution between atoms is mainly affected by the charge transfer between nuclear attractors. However, the valence basin center is located at this attractor position forming the bonds. In the case of bonds, attractors do not systematically localized on the bond midpoint and their localization depends on electronegativity differences between the atoms forming the bond and on the nature of the chemical environment. These attractor's positions are well defined by the mathematical properties of the ELF function in the framework of the theory of dynamical systems.

Finally, based on the coupled perturbed Hartree–Fock method, dipoles and higher hyperpolarizabilities have been globally and microscopically predicted. Local dipole contributions (dipolar polarization) have been shown to be useful to rationalize inductive polarization effects. It would be far easier to notice that the choice of the Y cations influences on the magnitude of the dipolar polarization. More the Y cation is heavy more it is polarizable. This behavior can be attributed to the charge deformation: more the density of electron is distorted more the electron are free to move. We found that the X lone pair electrons strongly interact with the surrounding Y-p orbitals, which are directly involved in the band gap formation, and the inter/intraband transitions giving rise to second harmonic generation properties.

## Acknowledgment

We would like to thank MALTA Consolider Team and Departamento de Química Física y Analítica, Universidad de Oviedo (Spain), especially, Professor J. M. Recio for giving us access to the computational facilities. Also we would like to thank Professor Ángel Martín Pendás for its appreciate discussion and help. A. H. R acknowledge the CENTEM project, reg. no. CZ.1.05/2.1.00/03.0088, cofunded by the ERDF as part of the Ministry of Education, Youth and Sports OP RDI programme and, in the follow-up sustainability stage, supported through CENTEM PLUS (LO1402) by financial means from the Ministry of Education, Youth and Sports under the National Sustainability Programme I.

## References

- [1] S. Schorr, *Sol. Energy Mater. Sol. Cells* 95 (2011) 1482.
- [2] C. Quemard, F. Smetkala, V. Couderc, A. Barthelemy, J. Lucas, *J. Phys. Chem.*

- Solids 62 (2001) 1435.
- [3] R.F.W. Bader, *Atoms in Molecules: A Quantum Theory*, Oxford University Press, Oxford, 1990.
- [4] R.F.W. Bader, P.M. Beddall, P.E. Cade, *J. Am. Chem. Soc.* 93 (13) (1971) 3095–3107.
- [5] K.E. Laidig, R.F.W. Bader, *J. Chem. Phys.* 93 (1990) 7213.
- [6] A.D. Becke, K.E. Edgecombe, *J. Chem. Phys.* 92 (1990) 5397.
- [7] B. Silvi, A. Savin, *Nature* 371 (1994) 683.
- [8] J. Pilmé, J.-P. Piquemal, *J. Comput. Chem.* 29 (2008) 1440.
- [9] B. Silvi, R.J. Gillespie, C. Gatti, 9.07-Electron Density Analysis. (In *Comprehensive Inorganic Chemistry II*, second ed., Poepelmeier, J. R., Elsevier, Amsterdam, 2013, pp. 187–226.
- [10] L.M. Peter, *Phil. Trans. R. Soc. A* 369 (2011) 1840.
- [11] T.K. Todorov, K.B. Reuter, D.B. Mitzi, *Adv. Mater.* 22 (2010) 20.
- [12] S. Chen, X.G. Gong, A. Walsh, S.-H. Wei, *Appl. Phys. Lett.* 94 (2009) 4.
- [13] D.M. Bishop, *Rev. Mod. Phys.* 62 (1990) 343.
- [14] D. Burland, *Chem. Rev.* 94 (1994) 1.
- [15] H.S. Nalwa, S. Miyata, *Nonlinear Optics of Organic Molecules and Polymers*, CRC Press, Boca Raton, 1997.
- [16] M.V. Putz, *Int. J. Quantum Chem.* 105 (2005) 1.
- [17] M.V. Putz, *Int. J. Mol. Sci.* 9 (2008) 1050.
- [18] A. Savin, O. Jepsen, J. Flad, L.K. Andersen, H. Preuss, H.G. von Schnering, *Angew. Chem. Int. Ed. Engl.* 31 (1992) 187.
- [19] J. Pilmé, E. Renault, A. Tahra, G. Montavon, N. Galland, *J. Chem. Theory Comput.* 8 (2012) 2985–2990.
- [20] R.J. Gillespie, R.S. Nyholm, *Quart. Rev.* 11 (1957) 339.
- [21] S. Raub, G. Jansen, *Theor. Chem. Acc.* 106 (3) (2001) 223–232.
- [22] P.L.A. Popelier, *Atoms in Molecules: An Introduction*, Prentice-Hall, Harlow, U. K, 2000.
- [23] B. de Courcy, L.G. Pedersen, O. Parisel, N. Gresh, B. Silvi, J. Pilmé, J.-P. Piquemal, *J. Chem. Theory Comput.* 6 (4) (2010) 1048–1063.
- [24] Elk FP-LAPW code, Kay Dewhurst, Sangeeta Sharma, Lars Nordstrom, Francesco Cricchio, Fredrik Bultmark, Hardy Gross, Claudia Ambrosch-Draxl, Clas Persson, Christian Brouder, Rickard Armiento, Andrew Chizmeshya, Per Anderson, Igor Nekrasov, Frank Wagner, Fateh Kalarasse, Jurgen Spitaler, Stefano Pittalis, Nektarios Lathiotakis, Tobias Burnus, Stephan Sagmeister, Christian Meisenbichler, Sebastian Lebegue, Yigang Zhang, Fritz Kormann, Alexey Baranov, Anton Kozhevnikov, Shigeru Suehara, Frank Essenberg, Antonio Sanna, Tyrel McQueen, Tim Baldsiefen, Marty Blaber, Anton Filanovich, Torbjorn Bjorkman <http://elk.sourceforge.net/>.
- [25] J.P. Perdew, A. Ruzsinszky, G.I. Csonka, L.A. Constantin, X. Zhou, O.A. Vydrov, G.E. Scuseria, and K. Burke, *Rev. Mod. Phys.* 100, 136406 (2008); *ibid.* 102, 039902 (2009).
- [26] F. Tran, P. Blaha, *Phys. Rev. Lett.* 102 (2009) 226401.
- [27] E. Engel, S.H. Vosko, *Phys. Rev. B* 47 (1993) 13164.
- [28] G. Kresse, D. Joubert, *Phys. Rev. B* 59 (1999) 1758.
- [29] D. Kozłowski, J. Pilmé, *J. Comput. Chem.* 32 (2011) 3207.
- [30] B.R. Pamplin, *J. Phys. Chem. Solids* 25 (1964) 675.
- [31] T.K. Todorov, K.B. Reuter, D.B. Mitzi, *Adv. Mater.* 22 (2010) E156.
- [32] A. Otero-de-la Roza, D. Abbasi-Pérez, V. Luaña *Comput. Phys. Commun.* 182 (2011) 2232.
- [33] H.-R. Liu, S. Chen, Y.-T. Zhai, H.J. Xiang, X.G. Gong, S.-H. Wei, *J. Appl. Phys.* 112 (093717) (2012).
- [34] H. Matsushita, T. Ichikawa, A. Katsui, *J. Mater. Sci.* 40 (2005) 2003.
- [35] S. Ahn, S. Jung, J. Gwak, A. Cho, K. Shin, K. Yoon, D. Park, H. Cheong, J.H. Yun, *Appl. Phys. Lett.* 97 (2010) 021905.
- [36] M. Ford, Q. Guo, R. Agrawal, H.W. Hillhouse, *Chem. Mater.* 23 (2011) 2626.
- [37] V. Parasyuk, L.V. Piskach, Y.E. Romanyuk, I.D. Olekseyuk, V.I. Zaremba, V.I. Pekhnyo, *J. Alloys Compd.* 397 (2005) 85.
- [38] S. Levchenko, A. Nateprov, V. Kravtsov, M. Guc, A. Pérez-Rodríguez, V. Izquierdo-Roca, X. Fontané, E. Arushanov, *Opt. Express* 22 (2014) A1936.
- [39] X. He, H. lieShen, *Phys. B* 406 (2011) 4604–4607.
- [40] X. He, H. lieShen, *Phys. Scr.* 85 (2012) 035302.
- [41] S. Bensalem, M. Chegaar, D. Maouche, A. Bouhemadou, *J. Alloys Compd.* 589 (2014) 137–142.
- [42] W. Voigt, *Lehrbuch der Kristallphysik*, Teubner, Leipzig, 1928.
- [43] A. Reuss, *Z. Angew. Math. Mech.* 9 (1929) 49.
- [44] I.R. Shein, A.L. Ivanovskii, *Scr. Mater.* 59 (2008) 1099.
- [45] Y. Zhang, L. Xi, Y. Wang, J. Zhang, P. Zhang, W. Zhang, *Comput. Mater. Sci.* 108 (2015) 239–249.
- [46] J.L.P. Hughes, J.E. Sipe, *Phys. Rev. B* 53 (1996) 10751.
- [47] S.N. Rashkeev, W.R.L. Lambrecht, B. Segall, *Phys. Rev. B* 57 (1998) 9705.
- [48] S. Sharma, J.K. Dewhurst, C. Ambrosch-Draxl, *Phys. Rev. B* 67 (2003) 165332.
- [49] M. Dahmani, T. Ouahrani, M. Mebrouki, A.H. Reshak, *Mater. Sci. Semicond. Process* 27 (2014) 433.
- [50] J. Contreras-García, A. Martín Pendás, J.M. Recio, *J. Phys. Chem. B* 112 (32) (2008) 9787–9794.
- [51] J. Contreras-García, A. Martín Pendás, J.M. Recio, B. Silvi, *J. Chem. Theory Comput.* 5 (1) (2009) 164–173.
- [52] R. Orlando, M. Ferrero, M. Rérat, B. Kirtman, R. Dovesi, *J. Phys. Chem.* 131 (2009) 184105.